The Electron Transfer Process in Mixed Valence Compounds with a Low-lying Energy Bridge in Different Oxidation States

Yu-ying Yang, Xiao-quan Zhu, Jean-pierre Launay, Cheng-bin Hong, Shao-dong Su, Yue-hong Wen, Xin-tao Wu, Tian-lu Sheng

The Electron Transfer Process in Mixed Valence Compounds with a Low-lying Bridge in Different Oxidization States

Yu-Ying Yang, Xiao-Quan Zhu, Jean-Pierre Launay, Cheng-Bin Hong, Shao-Dong Su, Yue-Hong Wen, Xin-Tao Wu and Tian-Lu Sheng

ABSTRACT: To understand electron transfer process with hopping or superexchange mechanisms is very important for the design of novel electron transfer materials. In this work the mixed valent compounds with the isocyanometal-ligand bridge in different oxidation states as models for the investigation of electron transfer process. Thus, we have designed and synthesized a series of trimetallic isocyanidometal-bridged compounds $[CpMe_x(dppe)Fe(\mu\text{-}CN)Ru(dmap)_4(\mu\text{-}NC)Fe(dppe)CpMe_x]^{n+}[PF_6]_n$ ($\mathbf{N}^{n+}[PF_6]_n$) (x = 0, 1, 3, 4 and 5, N = 1 - 5; n = 2 - 4). $\mathbf{N}^{3+}[PF_6]_3$ and $\mathbf{N}^{4+}[PF_6]_4$ are the one- and two-electron oxidation products of $\mathbf{N}^{2+}[PF_6]_2$, respectively. All the compounds have been fully characterized including by single-crystal X-ray diffraction structure analysis excepting for $\mathbf{1}^{4+}$ and $\mathbf{2}^{4+}$. The tri- and tetra-valent compounds $\mathbf{N}^{3+}[PF_6]_3$ and $\mathbf{N}^{4+}[PF_6]_4$ possess a low-lying cyanidometal-bridge which are lower and slightly higher than the terminal metal centers, respectively. The spectral data indicate that all the trivalent compounds are highly delocalized, while the degree of electron delocalization of tetravalent compounds increases as the donor becomes stronger. The electron transfer potential energy surfaces (PESs) of $\mathbf{N}^{3+}$ and $\mathbf{N}^{4+}$ were constructed by the three-state model analysis. The ground state PESs of the trivalent compounds shows that the minimums of the two degenerate excited mixed valence states overlay with the bridge ground state, which well explains the fact that the bridge-state and mixed-valence states are simultaneous observed on the IR timescale. The PESs results show the hopping mechanism is dominant for the ET process of all the trivalent compounds $\mathbf{N}^{3+}[PF_6]_3$. For the ET process of the tetravalent compounds $\mathbf{N}^{4+}[PF_6]_4$, however, both the hopping and superexchange mechanisms may coexist and the hopping mechanism may be more favored as the donor becomes stronger. For $\mathbf{1}^{4+}$ with the weakest electron donor both the hopping and superexchange mechanisms are present. For $\mathbf{5}^{4+}$ with the strongest electron donor, however, the hopping mechanism is complete dominant for the ET process.

Introduction

Electron transfer (ET) exists in nature and plays an important role in the physical, chemical, biological and material sciences.[1-5] Mixed-valence (MV) compounds with two (or more) redox centers in different oxidation states such as $[M^{n+}\text{-}B\text{-}M^{n+1}]$ in which M is metal center or metal cluster and B is conjugated organic or metallo-bridging ligand, are ideal model systems for the fundamental investigation of the ubiquitous ET processes.[6-7] Since the Creutz−Taube ion $[(NH_3)_5Ru\text{-pyrazine-}Ru(NH_3)_5]^{5+}$ (Chart 1a) was discovered,[8] much efforts have been devoted to investigate the influencing factors of ET, such as distance between the two redox centers and state level of the bridge.[9-12] The bridge state level affects the ET significantly. In previous studies, the dinuclear MV complexes with two “Cp*Fe(dppe)” redox center (Chart 1b) can transition from localized to delocalized MV complexes when the bridging-ligand was changed.[13-14] The triarylamine redox systems (Chart 1c) also show a similar result.[15-17] Besides, Baraldo and coworkers made great efforts to control the ET process by changing the linker (Chart 1d).[18-19] In these studies, it seems that the electron is more delocalized when the state level of the bridge becomes lower. Nelsen et al. proposed

that the zero-driving force thermal ET reaction, in which the small energy difference between the bridge and the redox centers, will significantly lower the ET barrier, and the energy gap from A^+-B-D to A-B^+-D is very small.[20] Such a bridge can lower the ET activation energy, as shown in Figure 1b. However, most of the investigated compounds possess a higher bridge state level than the redox centers. Only a few samples with a low-lying bridge state have been discussed, as shown in Figure 1a.[12, 17, 21] In this situation, A-B^+-D is the ground state and the A^+-B-D and A-B-D^+ are the excited state. Such a compound, the charge is located in bridge, is thought to be a mixed-valence character compound.[12] To date, however, no report has been appeared that how the strength of donor affect the ET process in such a situation.

Chart 1. Some models of the MV compounds

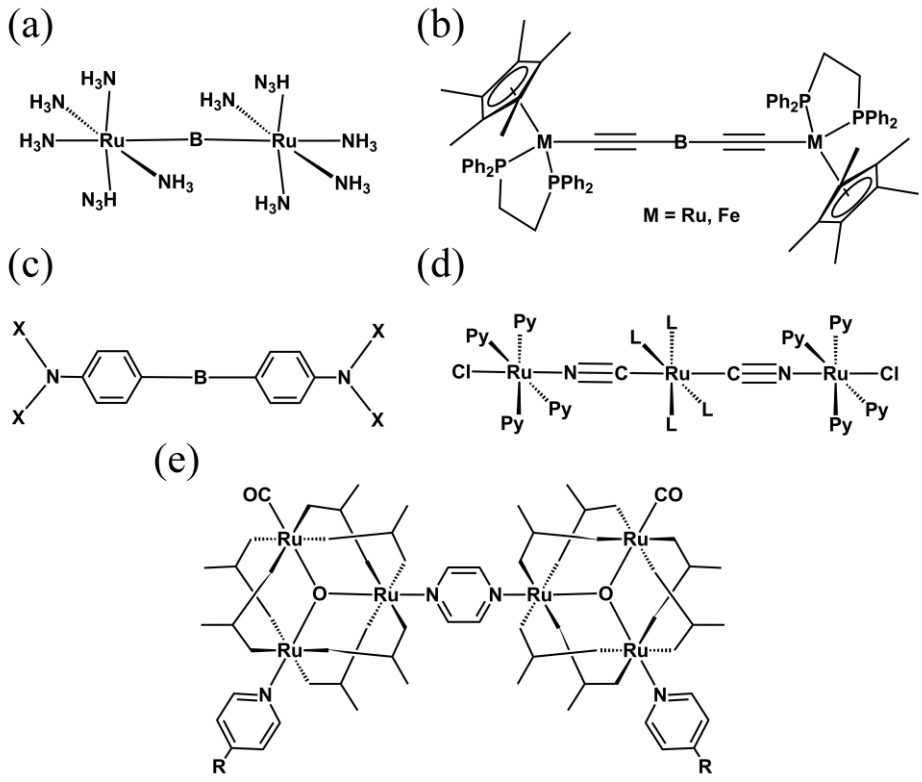

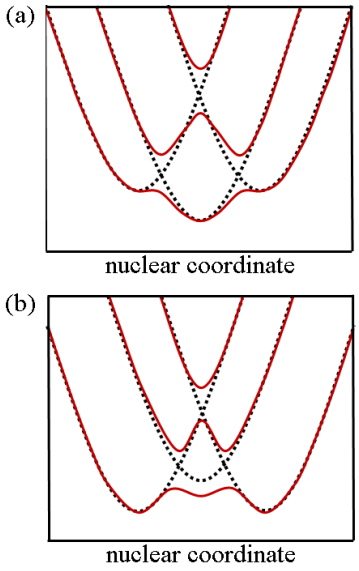

Figure 1 Diabatic (dashed lines) and adiabatic (solid lines) potential energy surfaces for the three-state system with low-lying bridge state which is (a) lower than the minimums of mixed-valence states; (b) higher than the minimums of mixed-valence states but lower than the crossing point of the diabatic mixed-valence states.

The strength of the electron donor is one of the key factors on electron delocalization. Clifford P. Kubiak and coworkers have reported a series of Ru_3O-based MV compounds (Chart 1 e).[22-23] The electron-donating ability and redox potential of the Ru_3O cluster are tuned by the pyridine ligands. The investigation showed that the strong donor of 4-dimethylaminopyridine can strengthen electron communication, resulting in electron delocalization on the IR timescale. Our previous studies have shown that the electron-donating group can tune the electronic communication between two metal centers.[24-25] The crystallographic data and the TDDF/DFT results indicate that, in a stronger donor compound, the electron density distributes more evenly, and the metallic dπ orbitals are more efficient mixing.

In this work, we focus on better understanding how the strength of donor affect the ET process when the compound possesses a low-lying bridge in the cases as shown in Figure 1. Previous studies had shown that the isocyanidometal-bridge -CN-M-NC- can lower state level of the metallo-bridge.[21, 26] By this in mind, we have designed and synthesized a series of isocyanidometal-bridged compounds (Figure 2). An oxidizable metal isocyanide fragment bridges two redox centers of $CpMe_xFe(dppe)$ (x = 0, 1, 3, 4, 5; Cp = cyclopentadienyl, $CpMe_1$ = 1-methyl-cyclopentadienyl, $CpMe_3$ = 1, 2, 4-triamethyl-1,3-cyclopentadienyl, $CpMe_4$ = 1, 2, 3, 4-tetramethyl-1,3-cyclopentadienyl, $CpMe_5$ = 1, 2, 3, 4, 5-pentamethyl-cyclopentadienyl) fragments, resulting in five compounds $[CpMe_xFe(dppe)CNRu(dmap)_4NC(dppe)FeCpMe_x]^{2+}$, $\mathbf{N}^{2+}$ (N = **1**, n = 0; N = **2**, x = 1; N = **3**, x = 3; N = **4**, x = 4; N = **5**, x = 5; dppe = 1,2-bis-(diphenylphosphino)ethane; dmap = 4-dimethylamino-pyridine). The donor strength can be tuned by the substituents of the Cp ring. First, the five divalent compounds were oxidized into trivalent with a Fe^{II}-CN-Ru^{III}-NC-Fe^{II} construction, $\mathbf{N}^{3+}$. All the trivalent compounds are mixed-valence character compounds which possess a low-lying bridge of Figure 1a. Furthermore, the trivalent MV compounds could be oxidized into the tetravalent MV compounds $\mathbf{M}^{4+}$ (Fe^{III}-CN-Ru^{III}-NC-Fe^{II}). In contrast with the trivalent compounds, the tetravalent compounds are symmetrical MV compounds with a low-lying bridge of Figure 1b, as confirmed by the fact that the minimum of the bridge state is higher than that of the mixed-valence states but lower than the crossing point (λ/4) of the diabatic mixed-valence states (see below). The three-state model are applied to analyze the ET

process of the trivalent $\mathbf{M^{3+}}$ and tetravalent $\mathbf{M^{4+}}$ MV compounds**.**

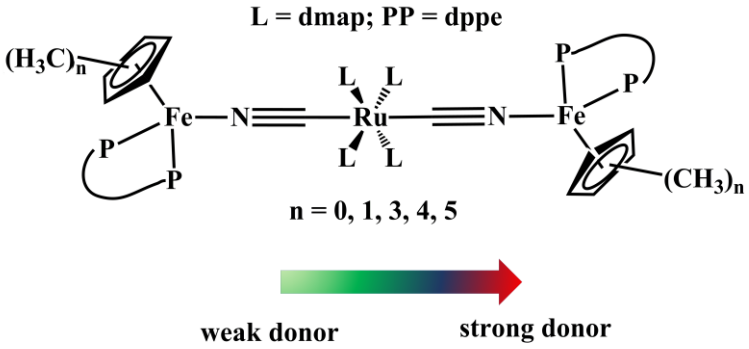

Figure 2. Isocyanidometal-bridged Fe-CN-Ru-NC-Fe compounds

RESULTS AND DISCUSSION

Electrochemistry

The cyclic voltammograms (CV) of the precursors $CpMe_x(dppe)FeCN$ (x = 0, 1, 3, 4 and 5) and compounds $\mathbf{1^{2+}}$–$\mathbf{5^{2+}}$ were performed in CH_3CN/0.1 M tetrabutylammonium hexafluorophosphate (TBAH), and the electrochemical data are summarized in Table 1 and Table S1, respectively. It can be seen from Table S1 that the electrochemical potential of the precursors $CpMe_x(dppe)FeCN$ decreases with increasing methyl groups of Cp, suggesting the electron-donating ability increases in the order Cp(dppe)FeCN < CpMe(dppe)FeCN < $CpMe_3$(dppe)FeCN < $CpMe_4$(dppe)FeCN < $CpMe_5$(dppe)FeCN.[27] For compounds $\mathbf{1^{2+}}$–$\mathbf{5^{2+}}$, the cyclic voltammograms all exhibit three chemically reversible one-electron oxidation waves (Figure S1). The first wave is attributed to the oxidation process of the bridging Ru center, while the last two waves are due to the oxidation processes of the two terminal Fe centers, suggesting the presence of electronic coupling between the two terminal Fe centers in compounds $\mathbf{1^{2+}}$–$\mathbf{5^{2+}}$.[28]

From Table 1, it is obvious that from $\mathbf{1^{2+}}$ to $\mathbf{5^{2+}}$ the potential separation (ΔE_2) between the two last waves increases and the potential separation (ΔE_1) between the first and the second waves decreases as the electron donor becomes stronger from CpFe(dppe) to $CpMe_5$Fe(dppe). For example, the CV of $\mathbf{1^{2+}}$ with the weakest electron donor CpFe(dppe) yields a smallest redox potential separation ΔE_2 of 0.12 V. But for the strongest electron donor $CpMe_5$Fe(dppe), compound $\mathbf{5^{2+}}$ shows the largest separation ΔE_2 of 0.38 V. Indeed, it has been reported that electrochemical separation is not a good quantitative measure of electronic coupling.[29-30] In cyanidometal-bridged system, however, the larger potential separation might be indicator of a stronger electron coupling.[18-19, 28, 31-33] The Ru_3O clusters system also show the similar result.[22-23, 34] Therefore, from the results of cyclic voltammograms it might be concluded for compounds $\mathbf{1^{2+}}$–$\mathbf{5^{2+}}$ that the electron coupling between the two terminal Fe increases as the electron-donating ability becomes stronger.

Based on the electrochemical measurement, upon one-electron oxidization the central Ru^{II} of compounds $\mathbf{1^{2+}}$–$\mathbf{5^{2+}}$ should be first oxidized into Ru^{III}. Thus, the reaction of $\mathbf{1^{2+}}$–$\mathbf{5^{2+}}$ with one equivalent of $Cp_2Fe(PF_6)$ gave rise to the MV compounds $\mathbf{1^{3+}}$-$\mathbf{5^{3+}}$ with the Fe^{II}-Ru^{III}-Fe^{II} arrangement. The tetravalent MV compounds $\mathbf{1^{4+}}$-$\mathbf{5^{4+}}$ with a Fe^{II}-Ru^{III}-Fe^{III} framework were obtained from further one-electron oxidation of $\mathbf{1^{3+}}$-$\mathbf{5^{3+}}$ with a stoichiometric amount of $AgPF_6$ or $NOPF_6$, respectively. Unfortunately, however, the isolation of $\mathbf{1^{4+}}$ and $\mathbf{2^{4+}}$ were unsuccessful due to their instability in the solid state that precluded us from obtaining their crystals for X-ray diffraction analysis and the Mössbauer spectral data.

Table 1. Half-wave potentials ($E_{1/2}$ vs Fc/Fc^+) and difference between the redox process (ΔE) of **1**-**5** from cyclic voltammetry at a scan rate of 0.1 V s^{-1}

	$E_{1/2}(1)$	$E_{1/2}(2)$	$E_{1/2}(3)$	ΔE_1	ΔE_2	[a]K_C
1	-0.25	0.45	0.57	0.70	0.12	104
2	-0.25	0.36	0.55	0.61	0.19	1557
3	-0.27	0.20	0.50	0.47	0.30	1.10×10^5
4	-0.27	0.16	0.49	0.43	0.33	3.51×10^5
5	-0.27	0.11	0.49	0.38	0.38	2.43×10^6

[a] The comproportionation constant K_C is calculated using ΔE_2, which is the potential separation of the two terminal Fe centers.

X-ray diffraction analysis

Compounds $\mathbf{1}^{2+}$–$\mathbf{5}^{2+}$, the one-electron oxidation products $\mathbf{1}^{3+}$-$\mathbf{5}^{3+}$ and the two-electron oxidation products $\mathbf{3}^{4+}$-$\mathbf{5}^{4+}$ were determined by X-ray diffraction with single crystal diffractometer ($\mathbf{1}^{2+}$–$\mathbf{5}^{2+}$, $\mathbf{1}^{3+}$-$\mathbf{4}^{3+}$ and $\mathbf{3}^{4+}$-$\mathbf{5}^{4+}$) or with synchrotron radiation ($\mathbf{5}^{3+}$). Crystallographic details and selected bond lengths and angles are summarized in Tables S2-S10 in the Supporting Information. In all the complexes, the two terminal $CpMe_x(dppe)Fe$ fragments are connected by the central isocyanidometal-bridge $(CN)Ru(dmap)_4(NC)$, showing a similar structure except for Cp ring. The structure of $\mathbf{5}^{2+}$ is shown in Figure 3, and the other structures are shown in Figures S2-S4 in the Supporting Information.

From Table 2, it can be seen that the average values for the Fe-P bond lengths of the trivalent compounds are longer than those of the corresponding divalent compounds, due to the π-back donation from the Fe center to the phosphorous atoms. However, it should be noted that the bond lengths of Fe-P (av. 2.1886(15)Å, 2.1887(14)Å) in $\mathbf{1}^{3+}$ change slightly compared with $\mathbf{1}^{2+}$ (av. 2.1930(12)Å, 2.1792(11)Å). This may result from the weakest donor CpFe(dppe) and the charge is more localized in the Ru centers of $\mathbf{1}^{3+}$ than others. Furthermore, the Fe1-C1, Fe2-C2, Ru-N1 and Ru-N2 bond lengths are shorter in $\mathbf{1}^{3+}$ (1.847(6)Å, 1.843(6)Å, 1.992(4)Å and 1.993(4)Å) than in $\mathbf{1}^{2+}$ (1.875(4)Å, 1.896(4)Å, 2.037(3)Å and 2.048(3)Å), suggesting the presence of electron delocalization along Fe^{II}-CN-Ru^{III}-NC-Fe^{II} which will strengthen the Fe-C_{CN} and Ru-N_{CN} bonds. Similar phenomena were also observed in M^{II}-C≡C-C≡C-M^{III}.[14, 35] The corresponding bond lengths in $\mathbf{2}^{3+}$-$\mathbf{5}^{3+}$ are similar to those in $\mathbf{1}^{3+}$ and shorter than those in $\mathbf{2}^{2+}$-$\mathbf{5}^{2+}$, respectively. These results suggest that for all the trivalent compounds there exists electron communication or delocalization between the center Ru^{III} and the terminal Fe^{II}.

For the tetravalent compounds, only the crystal data of $\mathbf{3}^{4+}$-$\mathbf{5}^{4+}$ were obtained. The structures of the compounds are in an unsymmetrical Fe^{II}-Ru^{III}-Fe^{III} arrangement. If the electron were localized, the Fe-P bond lengths of the two terminal $CpMe_n(dppe)Fe$ should be significantly different.[28, 32] It should be noted that for the MV compound $\mathbf{5}^{4+}$ the Fe-P bond lengths (av. 2.303(3) Å vs av. 2.295(3) Å) of the two terminal $CpMe_5(dppe)Fe$ are virtually indistinguishable within experimental error, suggesting that $\mathbf{5}^{4+}$ may be valence delocalized. Similarly, both the differences of the Fe-P bond lengths for $\mathbf{3}^{4+}$ (av. 2.2443(14) Å and av. 2.2356(18) Å) and $\mathbf{4}^{4+}$ (av. 2.253(3) Å and av. 2.269(2) Å) are 0.01 Å, being significantly smaller than the expected difference of ~0.06Å between Fe^{II}-P and Fe^{III}-P.[25, 36] Therefore, the investigation of the crystal data for the MV compounds may suggest the presence of the strong electron delocalization along Fe^{II}-CN-Ru^{III}-NC-Fe^{III}.

Table 2. Selected Bond Lengths for $\mathbf{1}^{n+}$ - $\mathbf{5}^{n+}$ (n = 2, 3) and $\mathbf{3}^{4+}$ - $\mathbf{5}^{4+}$

	[a]Fe1-P	[a]Fe2-P	Fe1-C1	Fe2-C2	Ru-N1	Ru-N2
$\mathbf{1}^{2+}$	2.1930(12)	2.1792(11)	1.875(4)	1.896(4)	2.037(3)	2.048(3)
$\mathbf{1}^{3+}$	2.1886(15)	2.1887(14)	1.847(6)	1.843(6)	1.992(4)	1.993(4)
$\mathbf{2}^{2+}$	2.1709(10)	–	1.882(4)	–	2.032(3)	–
$\mathbf{2}^{3+}$	2.1826(16)	2.1920(15)	1.854(6)	1.862(5)	2.015(5)	2.026(5)
$\mathbf{3}^{2+}$	2.1823(12)	2.1832(16)	1.902(5)	1.898(5)	2.047(4)	2.037(4)
$\mathbf{3}^{3+}$	2.2040(11)	2.2124(12)	1.888(4)	1.877(4)	2.040(3)	2.017(3)
$\mathbf{3}^{4+}$	2.2443(15)	2.2356(18)	1.900(5)	1.887(5)	2.006(4)	1.989(4)
$\mathbf{4}^{2+}$	2.1912(12)	2.1902(10)	1.904(4)	1.914(4)	2.064(3)	2.063(3)
$\mathbf{4}^{3+}$	2.2175(35)	–	1.890(12)	–	1.991(8)	–
$\mathbf{4}^{4+}$	2.2530(25)	2.2690(20)	1.896(8)	1.890(7)	2.008(6)	1.990(6)
$\mathbf{5}^{2+}$	2.2210(20)	2.2184(19)	1.917(6)	1.905(6)	2.068(5)	2.071(5)
$\mathbf{5}^{3+}$	2.2330(20)	–	1.863(7)	–	2.010(6)	–
$\mathbf{5}^{4+}$	2.3035(30)	2.2945(30)	1.908(9)	1.930(10)	2.012(7)	2.045(8)

a. average Fe-P bond length

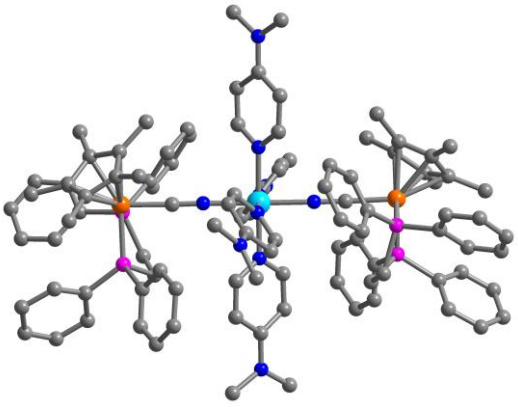

Figure 3. Molecular structure of $\mathbf{5}^{2+}$. Hydrogen atoms, $[PF_6]^-$ anions, and solvent molecules have been omitted for clarity. Light blue, Ru; orange, Fe; pink, P; gray, C; blue, N.

UV/Vis/NIR spectra

The UV/Vis/NIR spectra of five divalent compounds $\mathbf{1}^{2+}$-$\mathbf{5}^{2+}$ are similar and all of them contain only one absorption band at about 27600 cm^{-1} attributed to the MLCT absorption band of the $d\pi\rightarrow\pi^*$(dmap)[37] and $Fe^{II}\rightarrow$dppe transition,[28, 31-32] and do not exhibit any absorption band in Vis/NIR region (Figure S5).

Upon oxidation, the spectra of all the trivalent compounds display three new bands in the Vis-NIR region, and the band at about 27600 cm^{-1} disappears (Table 2 and Figure 4a). The two new bands at visible region

are attributed to the LMCT of the central Ru^{III} (π(dmap) → dπ(Ru^{III})), but the intensity of the absorption peak (about 3000 M^{-1} cm^{-1}) is significantly weaker than $Ru^{III}(dmap)_6$ (16000 ε / M^{-1} cm^{-1}).[18] This can be explained by the fact that there exists electron delocalization between the terminal Fe^{II} and the central Ru^{III}, which weakens the LMCT absorption from π(dmap) to dπ(Ru^{III}). The NIR spectra of $\mathbf{1}^{3+}$-$\mathbf{5}^{3+}$ display very sharp, asymmetric ET bands in the CH_2Cl_2 solution which are observed at 7732, 6708, 5715, 5479 and 5226 cm^{-1}, respectively. The maximum absorption wavelength of the trivalent compounds shows gradually redshift with the gradually increasing electron-donating $CpMe_x$(dppe)Fe from $\mathbf{1}^{3+}$ to $\mathbf{5}^{3+}$. As the donor becomes stronger, the state level is lower. Because the trivalent compounds have a low-lying bridge (Figure 1a), the energy difference ΔG will become smaller as the donor becomes stronger, resulting in a lower energy of the photo-induced ET process.

The tetravalent compounds also show strong NIR absorption bands (Figure 4b). The NIR bands of all the tetravalent compounds appear around 6000 cm^{-1} (Table 2). With the Fe^{II}-Ru^{III}-Fe^{III} structure of the MV compounds $\mathbf{1}^{4+}$-$\mathbf{5}^{4+}$, the Ru^{III} bridge is also an electron acceptor. The ET process undergoes a three-center way. Thus, the band in the NIR region is the sum of MBCT and IVCT. The bands in the visible region could be attributed to LMCT of the central Ru^{III} fragment, just like those in the trivalent compounds.

The UV−vis−NIR spectra obtained from the TD-DFT calculations of the trivalent compounds and their oxidized forms are shown in Figure S16-25. The computed NIR absorptions are in good agreement with the experimental absorption. For $\mathbf{1}^{3+}$, the NIR band at λ_{max} of 1196 nm mainly arises from the electronic transition from the highest occupied spin−orbital (HOSO)-250β to the lowest unoccupied spin orbital LUSO-253β (92%). The 250β spin orbital is dominated by the electronic population on the two Fe^{II} centers. The IVCT absorption is the ET process from the two terminal Fe^{II} centers to the central Ru^{III} of the bridge. The NIR bands of $\mathbf{2}^{3+}$-$\mathbf{5}^{3+}$ originate from the transition between the delocalized electronic levels, as shown in Figure S17-20. On the other hand, the computed NIR absorptions of $\mathbf{3}^{4+}$-$\mathbf{5}^{4+}$ originate from the orbital with more evenly distributed electronic population to an anti bonding LUSO orbital.

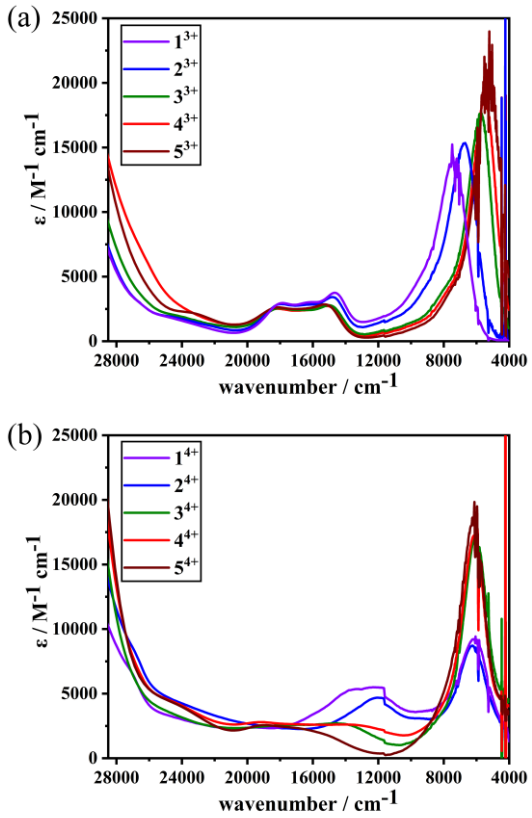

Figure 4. (a) Vis/NIR spectrum of all the trivalent compounds in CH_2Cl_2; (b) Vis/NIR spectrum of all the tetravalent compounds in CH_2Cl_2.

Table 3. Optical data for the IV-CT band of $\mathbf{1}^{3+}$ – $\mathbf{5}^{3+}$ and $\mathbf{1}^{4+}$ – $\mathbf{5}^{4+}$ in CH_2Cl_2.

	CT ν / cm^{-1}	CT ν / cm^{-1}		IVCT ν / cm^{-1}	IVCT ν / cm^{-1}
$\mathbf{1}^{3+}$	7732	14285	$\mathbf{1}^{4+}$	6167	9239
$\mathbf{2}^{3+}$	6708	15337	$\mathbf{2}^{4+}$	6235	8739
$\mathbf{3}^{3+}$	5715	17660	$\mathbf{3}^{4+}$	6012	17215
$\mathbf{4}^{3+}$	5479	18786	$\mathbf{4}^{4+}$	6112	17292
$\mathbf{5}^{3+}$	5226	20297	$\mathbf{5}^{4+}$	6172	18191

IR spectra

The IR tests for all the divalent compounds were performed in solid state, because those compounds are easily oxidized in the solution. All of those compounds exhibit a strong cyanide stretching vibration absorption. The IR spectra of trivalent and tetravalent compounds were recorded in solution. The ν(CN) bands of the compounds are summarized in Tables 4 and S11. In addition, the IR spectra only with ν(CN) bands of the trivalent compounds and the tetravalent compounds in solution are compared in Figure 6, Figure S26 and Figure 10, Figure S29-S31, respectively.

Upon oxidation, the IR spectra of $\mathbf{1}^{3+}$ and $\mathbf{2}^{3+}$ exhibit two cyanide stretching vibration absorptions at 2055 and 2008 cm^{-1}, 2055 and 1998 cm^{-1}, respectively (Figure S26). Unlike $\mathbf{1}^{3+}$ and $\mathbf{2}^{3+}$, the IR spectra of the other three trivalent compounds $\mathbf{3}^{3+}$, $\mathbf{4}^{3+}$ and $\mathbf{5}^{3+}$ displays three bands. The strong ν(CN) bands of $\mathbf{1}^{3+}$ and $\mathbf{2}^{3+}$ are not Gaussian shape and can be fitted by two bands. As the donor becomes stronger, the band in high wavenumber becomes stronger (see Figure 5). The low energy ν(CN) bands are attributed to the symmetric structure (Fe^{II}-CN-Ru^{III}-NC-Fe^{II}), in which the charge is localized in Ru. The two high energy bands could be attributed to the ET state (Fe^{III}-CN-Ru^{II}-NC-Fe^{II} or Fe^{II}-CN-Ru^{II}-NC-Fe^{III}), in which the charge is asymmetrically distributed between the two terminal centers. Therefore, the ET process over the three metal centers could be described as the manner: Fe^{III}-CN-Ru^{II}-NC-Fe^{II} ↔ Fe^{II}-CN-Ru^{III}-NC-Fe^{II} ↔ Fe^{II}-CN-Ru^{II}-NC-Fe^{III}, resulting in the superposition of the ν(CN) bands of the three states. For $\mathbf{1}^{3+}$, the charge mostly localizes in the Ru^{III}, so the symmetric ν(CN) band is dominant and the asymmetric bands are the weakest compared to the other trivalent compounds. As the donor $CpMe_xFe(dppe)$ becomes stronger, electron communication between the terminal Fe^{II} and the central Ru^{III} becomes stronger. The asymmetric ν(CN) bands of $\mathbf{5}^{3+}$ are the strongest, indicates that $\mathbf{5}^{3+}$ is the most delocalized one. In contrast, compound $\mathbf{1}^{3+}$ with the weakest donor is most localized on the IR timescale.

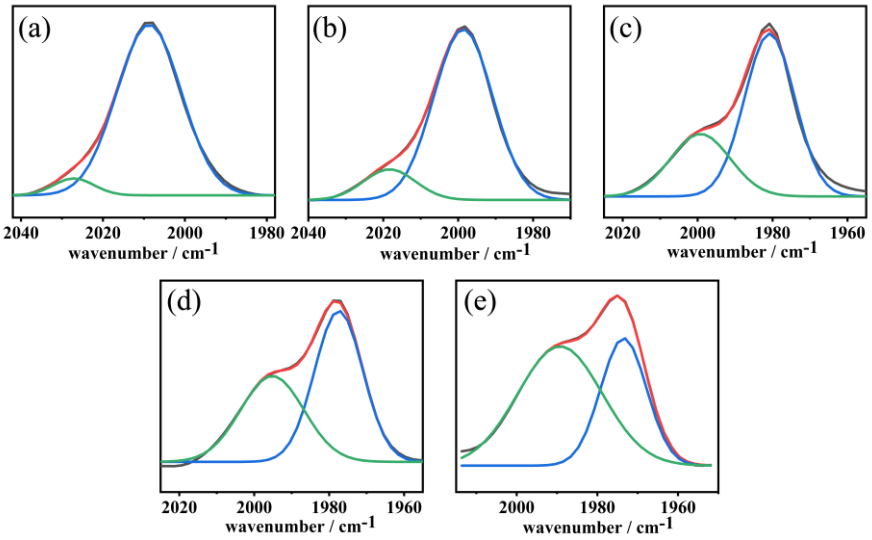

Figure 5. (a) the ν(CN) band of $\mathbf{1}^{3+}$(black line) and the sum of the fit bands (green line and blue line) is the red line(same as b, c, d and e); (b) the ν(CN) band of $\mathbf{2}^{3+}$;(c) the ν(CN) band of $\mathbf{3}^{3+}$ (d) the ν(CN) band of $\mathbf{4}^{3+}$ (e) the ν(CN) band of $\mathbf{5}^{3+}$.

For the tetravalent compounds with an asymmetric structure (Fe^{II}-CN-Ru^{III}-NC-Fe^{III}), the two bridging CN ligands should be in different environments when the MV compounds are localized. The IR absorption band shape of ν(CN) band depends on the electron coupling of the MV states. In many cases, the IR spectral features are usually used to investigate the ET process.[23, 38-43] The degree of overlapping of the ν(CN) band depends on the degree of electronic coupling between the two terminal Fe. If the intramolecular ET rate is fast on the IR timescale, the two ν(CN) bands for the Fe^{II}-CN-Ru^{III} and Ru^{III}-NC-Fe^{III} units will overlay into a single band. In contrast, if the ET rate is slower than the IR timescale, the two ν(CN) bands can be observed.[18, 23, 28, 44-45] As shown in Table 4, the IR spectra of $\mathbf{1}^{4+}$ and $\mathbf{2}^{4+}$ exhibit two ν(CN) bands, suggesting both the complexes could be classed into localized MV compounds on the IR timescale. In $\mathbf{3}^{4+}$, the two bands are very close. $\mathbf{4}^{4+}$ has a broad cyanide stretching vibration absorption, but two bands can still be

observed. The spectrum of $\mathbf{5}^{4+}$ exhibits only one absorption at 1961 cm^{-1}, the characteristic of delocalized MV systems, indicating the two CN are equivalent on the IR timescale.

Table 4 Summary of the ν(CN) of $\mathbf{[1\text{-}5]}^{n+}$ (n = 3, 4) in CH_2Cl_2

	ν(CN)		ν(CN)	k_{obs}
$\mathbf{1}^{3+}$	2055(w)	$\mathbf{1}^{4+}$	2006(m)	2.0×10^{10} s^{-1}
	2027(w)[a]		1976(m)	
	2008(vs)[a]			
$\mathbf{2}^{3+}$	2055(w)	$\mathbf{2}^{4+}$	2006(m)	5.0×10^{10} s^{-1}
	2018(w)[a]		1961(s)	
	1998(vs)[a]			
$\mathbf{3}^{3+}$	2055(w)	$\mathbf{3}^{4+}$	1979(m)	3.3×10^{11} s^{-1}
	1999(w)		1956(s)	
	1980(s)			
$\mathbf{4}^{3+}$	2055(w)	$\mathbf{4}^{4+}$	1957(m)[b]	1.7×10^{12} s^{-1}
	1995(m)		1978(m)[b]	
	1977(s)			
$\mathbf{5}^{3+}$	2055(w)	$\mathbf{5}^{4+}$	1961(m)	2.5×10^{12} s^{-1}
	1989(s)			
	1973(s)			

[a] those bands are obtained by fitting the strong ν(CN) band. [b] the ν(CN) band of $\mathbf{4}^{4+}$ is broad, and the two bands are obtained by fitting thev(CN) band.

^{57}Fe Mössbauer Spectroscopy

It has been known that ^{57}Fe Mössbauer spectroscopy can be used to monitor the ET rate.[44, 46-48] To further investigate the process of electron delocalization, zero-field variable-temperature ^{57}Fe Mössbauer spectra of the samples of $\mathbf{1}^{3+}$–$\mathbf{5}^{3+}$ and $\mathbf{3}^{4+}$–$\mathbf{5}^{4+}$ were performed. The quadrupole splitting (QS) and isomer shift (IS) parameters of $\mathbf{1}^{3+}$–$\mathbf{5}^{3+}$ and $\mathbf{3}^{4+}$–$\mathbf{5}^{4+}$ are given in Tables 5. For the purpose of comparison, ^{57}Fe Mössbauer spectra of $\mathbf{1}^{2+}$, $\mathbf{4}^{2+}$, $\mathbf{5}^{2+}$, $Cp^*(dppe)Fe^{II}CN$ and $[Cp^*(dppe)Fe^{III}CN](PF_6)$ were also measured at room temperature (Table S17). It can be seen that $\mathbf{1}^{2+}$, $\mathbf{5}^{2+}$ and $Cp^*(dppe)Fe^{II}CN$ show one typical quadrupole doublet with the parameters of QS about 1.90 $mm.s^{-1}$ for localized Fe^{II},[49-50] and $[Cp^*(dppe)Fe^{III}CN](PF_6)$ displays one typical quadrupole doublet for localized Fe^{III}.

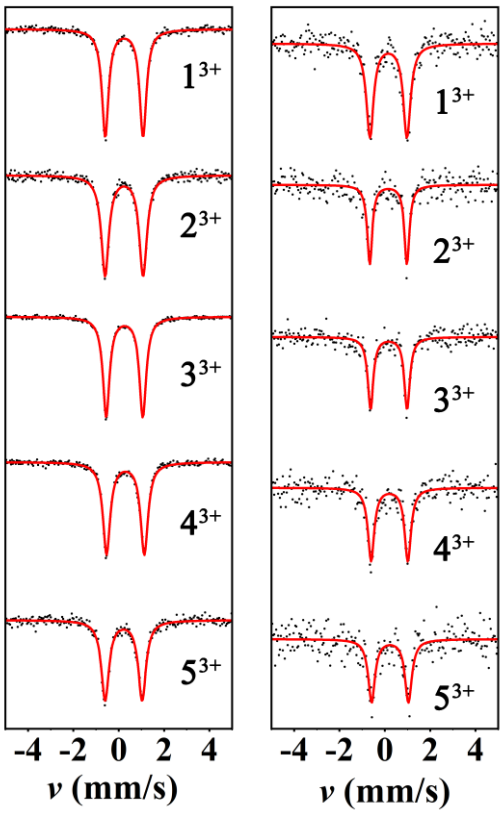

Figure 6 the ^{57}Fe Mössbauer spectra of $\mathbf{1}^{3+}$–$\mathbf{5}^{3+}$ at 10 K (left) and 300 K (right).

The spectra of $\mathbf{1}^{3+}$–$\mathbf{5}^{3+}$ exhibit only one quadrupole doublet, suggesting both the terminal iron centers are equivalent. The QS of all the trivalent compounds is about 1.65 mm.s^{-1} and is much smaller than those of localized Fe^{II} in divalent compounds $\mathbf{1}^{2+}$–$\mathbf{5}^{2+}$ and in the reported MV compound Fe^{II}-CN-Fe^{III}-NC-Fe^{II} (2.03 mm.s^{-1}),[49] but are close to that of the delocalized Fe reported for the same iron fragment,[50] suggesting the one quadrupole doublet of $\mathbf{1}^{3+}$–$\mathbf{5}^{3+}$ could be attributed to delocalized Fe. Lapinte and coworkers reported that the QS parameter of delocalized Fe^{II}-Fe^{III} compound is 1.32 mm.s^{-1}, smaller than those of $\mathbf{1}^{3+}$–$\mathbf{5}^{3+}$. Notably, however, the QS value of the delocalized Fe in $\mathbf{1}^{3+}$–$\mathbf{5}^{3+}$ is somewhat larger than the average one (1.337 mm/s) of Fe^{II} and Fe^{III}, this may be due to an incomplete charge transfer from Fe^{II} to Ru^{III}. Furthermore, this equivalence is not a function of the temperature, and the spectra recorded at 10 K all show the presence of only one type of iron, and the parameters are almost temperature independent (Figure 6 and Table 6). Based on those results, $\mathbf{1}^{3+}$–$\mathbf{5}^{3+}$ could be assigned to the delocalized compounds on the Mössbauer timescale.

For the tetravalent compounds, the ^{57}Fe Mössbauer spectra for $\mathbf{1}^{4+}$–$\mathbf{2}^{4+}$ were not obtained. The spectra (Figure S28-29) of $\mathbf{3}^{4+}$ and $\mathbf{4}^{4+}$ show two quadrupole doublets, while the $\mathbf{5}^{4+}$ has only one. For $\mathbf{3}^{4+}$ and $\mathbf{4}^{4+}$, two quadrupole doublets are observed: the first one with QS =1.66 mms^{-1} comparable to those of the trivalent compounds which are attributed to the delocalized Fe of Fe^{II}-Ru^{III}; the second one with QS = 0.68 mms^{-1}, which should be attributed to the two delocalized terminal iron ions.[44] Although $\mathbf{3}^{4+}$ and $\mathbf{4}^{4+}$ show the similar quadrupole doublets, it should be noted that the relative area of the delocalized Fe is different. $\mathbf{4}^{4+}$ has more delocalized component about 75.6% while $\mathbf{3}^{4+}$ is 61.3%. The spectrum of $\mathbf{5}^{4+}$ with one quadrupole doublet (QS = 0.69 mms^{-1}) indicates that $\mathbf{5}^{4+}$ is a fully delocalized species and the two terminal iron ions are equivalent. Even at 10 K, the spectrum of $\mathbf{5}^{4+}$ also shows one quadrupole doublet with QS = 0.60 mms^{-1}.

Table 5. ^{57}Fe Mössbauer Fitting Parameters for Selected Complexes

	T / K	IS (mm.s^{-1})	QS (mm.s^{-1})	Relative Area (%)
$\mathbf{1}^{3+}$	10	0.23	1.67	100
	300	0.15	1.63	100
$\mathbf{2}^{3+}$	10	0.23	1.68	100
	300	0.15	1.64	100
$\mathbf{3}^{3+}$	10	0.25	1.61	100
	300	0.17	1.61	100
$\mathbf{4}^{3+}$	10	0.29	1.66	100
	300	0.20	1.62	100
$\mathbf{5}^{3+}$	10	0.23	1.624	100
	300	0.21	1.631	100
$\mathbf{3}^{4+}$	300	0.27	1.67	38.7
		0.29	0.69	61.3
$\mathbf{4}^{4+}$	300	0.56	1.66	24.4
		0.49	0.68	75.6
$\mathbf{5}^{4+}$	10	0.27	0.60	100
	300	0.23	0.69	100

DISCUSSION

ET of trivalent compounds

The ET process of the trivalent compounds are analyzed by the three-centers model. Those compounds show a very intense and asymmetric NIR band. The analysis is based on the assumption that the NIR band consists of the bridge band. This assignment is feasible. First, the NIR bands of $\mathbf{1}^{3+}$–$\mathbf{5}^{3+}$ are asymmetrical and can be fitted by two or more bands. Secondly, the bridge center Ru^{II} of all the compounds will be oxidized first. So, those compounds have a low-lying bridge, and prefer to a bridge-mediated hopping ET process.[17, 21, 51-52] The analysis of electron transition is shown in Figure 7. ν_a and ν_b arise from the ground state to the first excited state [Fe^{II}-CN-Ru^{II}-NC-Fe^{III}] (or [Fe^{III}-CN-Ru^{II}-NC-Fe^{II}]) and the second excited state [Fe^{II}-CN-Ru^{II}-NC-Fe^{II}]$^{+*}$, respectively. ν_{IVCT} arises from the first excited state to the second excited state. Based on previous studies[12, 15, 17] and our analysis, the asymmetric NIR band is fitted by three Gaussian functions (Figure S6-10).

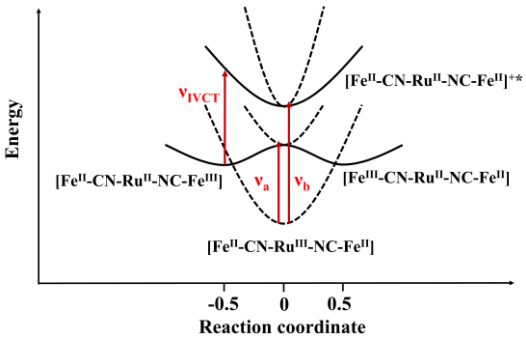

Figure 7. Schematic adiabatic potential energy curves for the trivalent compounds. The solid lines are shown in the asymmetric reaction coordinate, the electron transition process is ν_{IVCT}; the dashed line lines are shown in the symmetric reaction coordinate, which runs perpendicular to the asymmetric coordinate, the electron transition process is ν_a and ν_b.

It has been reported that the three-centers model is successful to be used to describe ET of the bridged MV complexes.[15, 53-56] Here, we use the optimized Launay-Coudret-Hortholary model,[7] to analysize the ET process of the trivalent and tetravalent MV complexes. The details about the model and the parameters are given in the supporting information. The parameters used for PES (potential energy surface) are listed in Table 6. The coupled adiabatic PES can be given by solving the determinant for the eigenvalues, E (equation 1 in the Supporting Information). The ground-state PESs of those compounds are given in Figure 8 and Figure S33.

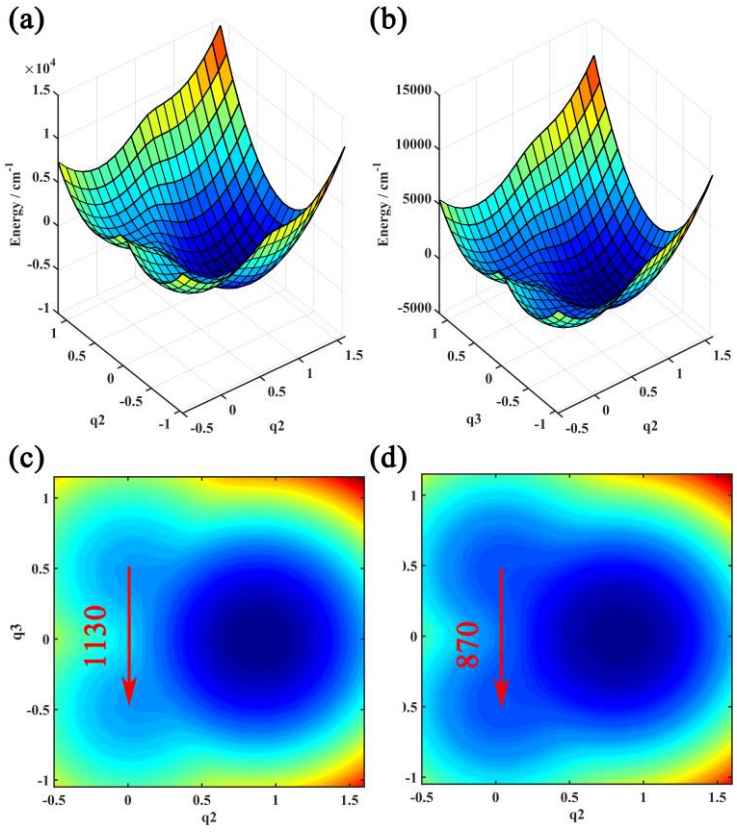

Figure 8. (a) the PES of $\mathbf{1}^{3+}$; (b) the PES of $\mathbf{5}^{3+}$; (c) the PES contour of $\mathbf{1}^{3+}$; (d) the PESs contour of $\mathbf{5}^{3+}$. The red arrow indicates the ET process between the two excited states.

As the PESs show, the two minimums in high energy are the excited states (Fe^{III}-Ru^{II}-Fe^{II} and Fe^{II}-Ru^{II}-Fe^{III}) of the trivalent compounds. However, the two minimums overlay with the ground state Fe^{II}-Ru^{III}-Fe^{II} and show a special minimum. Because of the low-lying bridge state level and strong electron coupling between Fe^{II} and Ru^{III}, the energy barrier becomes very small and even disappears (the $\Delta G^* = 0$). The new ground state is the superposition of the excited state and ground state. That is in good agreement with the above IR spectra that the bridge-state and mixed-valence states are simultaneous observed. As shown in the PES contour, although the PES of $\mathbf{1}^{3+}$ is smooth, the energy difference (ΔG^0) between the bridge and the donor is the largest, suggesting the excited states of $\mathbf{1}^{3+}$ are less stable. This can explain the fact that theν(CN) absorptions of Fe^{III}-CN-Ru^{II}-NC-Fe^{II} are the weakest (Figure 5). The PESs show that, as the methyl substituents of the Cp ring ligand increase, the electron-donating properties of the Fe^{II} become stronger and the ΔG^0 becomes smaller. So the excited states become more stable. Theν(CN) absorptions of excited state Fe^{III}-CN-Ru^{II}-NC-Fe^{II} become stronger.

Table 6. ET parameters for the analysis of three-state model of $\mathbf{1}^{3+}$-$\mathbf{5}^{3+}$

	λ	ΔG^0 / cm^{-1}	V_{12} / cm^{-1}
1^{3+}	11073	-5644	1586
2^{3+}	10263	-4918	1627
3^{3+}	9160	-3790	1619
4^{3+}	8716	-3466	1621
5^{3+}	8278	-3068	1643

ET of tetravalent compounds

We estimate the ET rate constants by analysis of ν(CN) band broadening in the IR spectra, and this method had been used for the determination of ET rate constants in MV systems.[23, 43, 45] The ν(CN) band simulations of all the tetravalent compounds were performed using the published software,[57] and the results are shown in Figure 10 and Figure S30-32. The observed rate constants (k_{obs}) are listed in Table 3. $\mathbf{5}^{4+}$ shows the fastest ET rate, $k_{obs} = 2.5 \times 10^{12}$ s^{-1}. As the donor becomes weaker, the ET rates of those compounds become slow gradually, $k_{obs} = 2.0 \times 10^{10}$ s^{-1} for $\mathbf{1}^{4+}$. Those results correspond to the Mössbauer spectral results that the tetravalent MV compound becomes more delocalization from $\mathbf{3}^{4+}$ to $\mathbf{5}^{4+}$ on the Mössbauer timescale.

The tetravalent compounds have a D-A_1^+-A_2^+ structure and the NIR band is the sum of MBCT and IVCT. The parameters used for three-state analyses were obtained by fitting the NIR band, the details are shown in Figure S11-15, Table S14-15. As the fitting results shown, the $\Delta G°$ is lower than the crossing point (λ/4) of the diabatic states, as shown in Figure 1b. The PESs are shown in Figures 9 and S34. For those compounds, $\Delta G°$ is lower than the crossing point of the diabatic states (1) and (3) as shown in Figure 1b, which can lower the ET barrier ΔG_{13}*. However, although the ΔG^0 of $\mathbf{1}^{4+}$ is the smallest, the ET rate is the slowest and the electron coupling is the smallest (952 cm^{-1}) due to the weaker donor of $CpFe^{II}$(dppe) than $CpMe_xFe^{II}$(dppe) (x = 1, 3, 4 and 5). The similar phenomenon that the weak donor is unbeneficial to ET was previously reported.[24-25, 58] The PES of $\mathbf{1}^{4+}$ (Figure 9a) has three minimums, and the PES contour (Figure 9c) shows that

the ET process has a high barrier. The yellow arrow indicates the ET path with superexchange mechanism should crosse a high energy barrier of about 1390 cm^{-1}. In contrast, the hopping way needs to overcome a lower energy. The attachment of methyl groups to the Cp ring lower the state level of the donor and the ΔG° becomes larger, but the strong donor strengthens electron coupling. The PESs of $\mathbf{3}^{4+}$-$\mathbf{5}^{4+}$ show the delocalized characteristic, and the high energy minimum has disappeared (Figure 9b and Figure S34), suggesting the presence of electron delocalization between Fe^{II} and Ru^{III}. For $\mathbf{3}^{4+}$-$\mathbf{4}^{4+}$, the ET process between the terminal metal centers should overcome an activation energy of 900 cm^{-1} for $\mathbf{3}^{4+}$ and 500 cm^{-1} for $\mathbf{4}^{4+}$. This is consistent with the results of their ^{57}Fe Mössbauer spectroscopy results that show the fully delocalized and the delocalized Fe^{II}-Ru^{III} components are 61.3% and 38.7% for $\mathbf{3}^{4+}$, and 75.6% and 24.4% for $\mathbf{4}^{4+}$, respectively. The PES shows that $\mathbf{5}^{4+}$ is a fully delocalized species, being consistent with all the spectroscopy data.

Table 7 ET parameters for analysis of three-state model of $\mathbf{1}^{4+}$-$\mathbf{5}^{4+}$

	λ	ΔG^0 / cm^{-1}	V_{12} / cm^{-1}
0	6844	802	952
1	7141	992	1127
3	7566	1593	1768
4	7681	1608	2180
5	7810	1678	3065

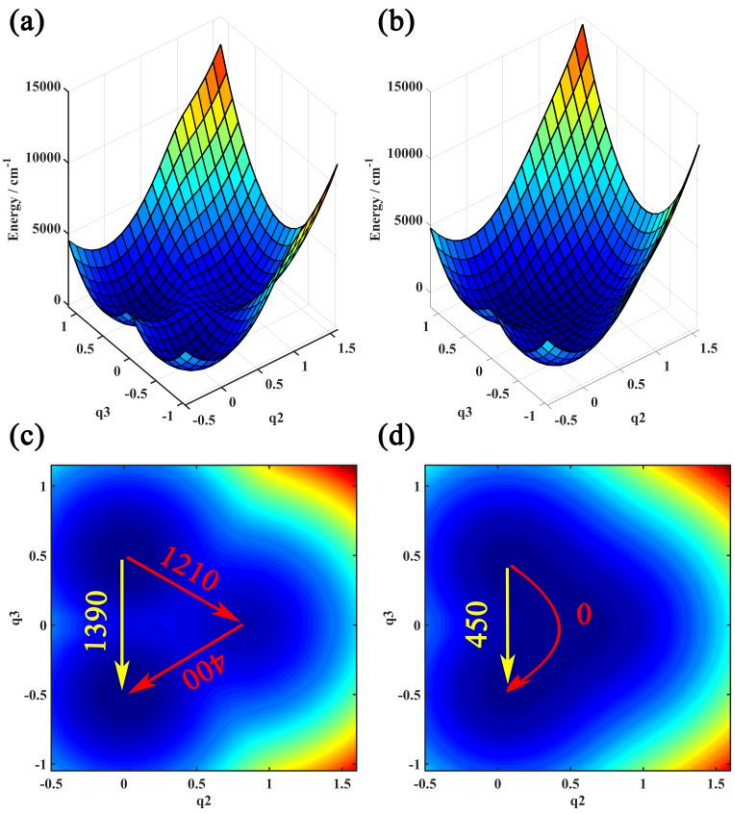

Figure 9 (a) the PESs of $\mathbf{1}^{3+}$; (b) the PESs of $\mathbf{5}^{3+}$; (c) the PESs contour of $\mathbf{1}^{3+}$; (d) the PESs contour of $\mathbf{5}^{3+}$.

The yellow arrow indicates the superexchange ET process; the red arrows indicate the hopping ET process.

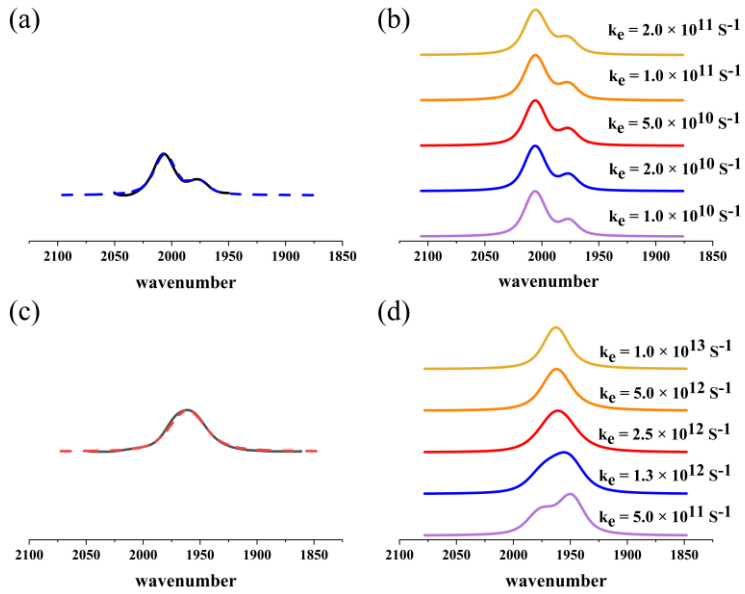

Figure 10. Comparison of observed (left) and simulated (right) stretching frequencies for the CN bonds in the tetravalent MV complexes. (a) black line: the observed result of $\mathbf{1}^{4+}$; blue line: the best simulated result of $\mathbf{1}^{4+}$. (b) the simulated result of $\mathbf{1}^{4+}$. (c) black line: the observed result of $\mathbf{5}^{4+}$; red line: the best simulated result of $\mathbf{5}^{4+}$. (d) the simulated result of $\mathbf{5}^{4+}$.

CONCLUSION

To investigate the electron transfer mechanism of mixed valence compounds in which the bridging ligand in mediating electronic interaction is low-lying, we have designed and synthesized a series of isocyanometal-bridged trimetallic compounds $\mathbf{1}^{n+}$ - $\mathbf{5}^{n+}$ (n = 2, 3 and 4) with the general formula of $[CpMe_x(dppe)Fe(\mu\text{-}CN)Ru(dmap)_4(\mu\text{-}NC)Fe(dppe)CpMe_x]^{n+}$ (x = 1-5), $\mathbf{1}^{3+}$ - $\mathbf{5}^{3+}$ and $\mathbf{1}^{4+}$ - $\mathbf{5}^{4+}$ are the one- and two-electron oxidized products of $\mathbf{1}^{2+}$ - $\mathbf{5}^{2+}$, respectively. All the compounds have been fully characterized including by single-crystal X-ray diffraction structure analysis excepting for $\mathbf{1}^{4+}$ and $\mathbf{2}^{4+}$. For the trivalent compounds $\mathbf{1}^{3+}$ - $\mathbf{5}^{3+}$, the energy level of the bridge state (Fe^{II}-Ru^{III}-Fe^{II}) is lower than that of the mixed valence states (Fe^{III}-Ru^{II}-Fe^{II} and Fe^{II}-Ru^{II}-Fe^{III}). The ground state PES of the trivalent compounds constructed by the three-state model analysis shows that the minimums of the two degenerate excited mixed valence states overlay with the ground state, resulting in the simultaneous observations of the bridge-state and mixed-valence states. The PES also shows that the ET barrier to the bridge-state is almost disappeared and is much lower than that of the direct superexchange pathway, suggesting the hopping mechanism is dominant for the ET process of all the trivalent compounds. Upon further one-electron oxidation of $\mathbf{1}^{3+}$ - $\mathbf{5}^{3+}$, the bridge state (Fe^{III}-Ru^{II}-Fe^{III}) level of $\mathbf{1}^{4+}$ - $\mathbf{5}^{4+}$ increases and is higher than that of the mixed valence states (Fe^{III}-Ru^{III}-Fe^{II} and Fe^{II}-Ru^{III}-Fe^{III}). The ground-state PES for the tetravalent compounds are also constructed from the spectral analysis. The PES shows both the hopping and superexchange mechanisms are present for $\mathbf{1}^{4+}$ with the weakest electron donor. As the donor becomes stronger, the hopping mechanism is more favored for the ET process of tetravalent compounds. For $\mathbf{5}^{4+}$ with the strongest electron donor, the hopping mechanism is complete dominant for the ET process. This study indicates that the sufficient low bridge state level has a more important effect on the ET process than other influencing factors. If the bridge state level is slightly higher than the terminal metal centers, both the hopping and superexchange mechanisms may

coexist, but the hopping mechanism may be more favored for the ET process if the donor becomes stronger. This may have implications in designing molecular electronic devices.

References:

1. Winkler, J. R.; Gray, H. B., Electron-Transfer in Ruthenium-Modified Proteins. *Chem Rev* **1992,** *92* (3), 369-379.
2. Koval, C. A.; Howard, J. N., Electron-Transfer at Semiconductor Electrode Liquid Electrolyte Interfaces. *Chem Rev* **1992,** *92* (3), 411-433.
3. Meng, Y. S.; Sato, O.; Liu, T., Manipulating Metal-to-Metal Charge Transfer for Materials with Switchable Functionality. *Angew Chem Int Edit* **2018,** *57* (38), 12216-12226.
4. Marcus, R. A.; Sutin, N., Electron transfers in chemistry and biology. *Biochimica et Biophysica Acta (BBA) - Reviews on Bioenergetics* **1985,** *811* (3), 265-322.
5. Zahler, C. T.; Zhou, H.; Abdolvahabi, A.; Holden, R. L.; Rasouli, S.; Tao, P.; Shaw, B. F., Direct Measurement of Charge Regulation in Metalloprotein Electron Transfer. *Angew Chem Int Ed Engl* **2018,** *57* (19), 5364-5368.
6. Heckmann, A.; Lambert, C., Organic Mixed-Valence Compounds: A Playground for Electrons and Holes. *Angew Chem Int Edit* **2012,** *51* (2), 326-392.
7. Launay, J. P.; Coudret, C.; Hortholary, C., Three-centers models for electron transfer through a bridge. 1. Potential energy surfaces. *J Phys Chem B* **2007,** *111* (24), 6788-6797.
8. Creutz, C.; Taube, H., A Direct Approach to Measuring Franck-Condon Barrier to Electron Transfer between Metal Ions. *Journal of the American Chemical Society* **1969,** *91* (14), 3988-3989.
9. Richardson, D. E.; Taube, H., Mixed-Valence Molecules - Electronic Delocalization and Stabilization. *Coordin Chem Rev* **1984,** *60* (Nov), 107-129.
10. Joss, S.; Burgi, H. B.; Ludi, A., Mixed-Valence Ruthenium Dimers - Molecular and Electronic-Structure of the Para-Benzoquinone Diimine Bridged Ion [(Nh3)5ru(Bqd)Ru(Nh3)5]5+ (Bqd= Para-Benzoquinone Diimine) and Its Relationship to the Creutz-Taube Ion. *Inorg Chem* **1985,** *24* (6), 949-954.
11. Launay, J.-P., Long-distance intervalence electron transfer. *Chem. Soc. Rev.* **2001,** *30* (6), 386-397.
12. Fox, M. A.; Le Guennic, B.; Roberts, R. L.; Brue, D. A.; Yufit, D. S.; Howard, J. A. K.; Manca, G.; Halet, J.-F.; Hartl, F.; Low, P. J., Simultaneous Bridge-Localized and Mixed-Valence Character in Diruthenium Radical Cations Featuring Diethynylaromatic Bridging Ligands. *Journal of the American Chemical Society* **2011,** *133* (45), 18433-18446.
13. Ibn Ghazala, S.; Paul, F.; Toupet, L.; Roisnel, T.; Hapiot, P.; Lapinte, C., Di-organoiron mixed valent complexes featuring "(eta2-dppe)(eta5-C5Me5)Fe" endgroups: smooth class-III to class-II transition induced by successive insertion of 1,4-phenylene units in a butadiyne-diyl bridge. *J Am Chem Soc* **2006,** *128* (7), 2463-76.
14. Halet, J. F.; Lapinte, C., Charge delocalization vs localization in carbon-rich iron mixed-valence complexes: A subtle interplay between the carbon spacer and the (dppe)Cp*Fe organometallic electrophore. *Coordin Chem Rev* **2013,** *257* (9-10), 1584-1613.
15. Lambert, C.; Noll, G.; Schelter, J., Bridge-mediated hopping or superexchange electron-transfer processes in bis(triarylamine) systems. *Nat Mater* **2002,** *1* (1), 69-73.
16. Lambert, C.; Nöll, G., The Class II/III Transition in Triarylamine Redox Systems. *Journal of the American Chemical Society* **1999,** *121* (37), 8434-8442.
17. Lambert, C.; Amthor, S.; Schelter, J., From Valence Trapped to Valence Delocalized by Bridge

State Modification in Bis(triarylamine) Radical Cations: Evaluation of Coupling Matrix Elements in a Three-Level System. *The Journal of Physical Chemistry A* **2004,** *108* (31), 6474-6486.

18. Pieslinger, G. E.; Albores, P.; Slep, L. D.; Baraldo, L. M., Class III Delocalization in a Cyanide-Bridged Trimetallic Mixed-Valence Complex. *Angewandte Chemie International Edition* **2014,** *53* (5), 1293-1296.

19. Pieslinger, G. E.; Albores, P.; Slep, L. D.; Coe, B. J.; Timpson, C. J.; Baraldo, L. M., Communication between Remote Moieties in Linear Ru-Ru-Ru Trimetallic Cyanide-Bridged Complexes. *Inorg Chem* **2013,** *52* (6), 2906-2917.

20. Nelsen, S. F.; Ismagilov, R. F.; Powell, D. R., Effects of bridge redox state levels on the electron transfer and optical properties of intervalence compounds with hydrazine charge-bearing units. *Journal of the American Chemical Society* **1998,** *120* (8), 1924-1925.

21. Bignozzi, C. A.; Roffia, S.; Chiorboli, C.; Davila, J.; Indelli, M. T.; Scandola, F., Oligomeric Dicyanobis(Polypyridine)Ruthenium(Ii) Complexes - Synthesis and Spectroscopic and Photophysical Properties. *Inorg Chem* **1989,** *28* (24), 4350-4358.

22. Glover, S. D.; Goeltz, J. C.; Lear, B. J.; Kubiak, C. P., Inter- or intramolecular electron transfer between triruthenium clusters: we'll cross that bridge when we come to it. *Coordin Chem Rev* **2010,** *254* (3-4), 331-345.

23. Ito, T.; Hamaguchi, T.; Nagino, H.; Yamaguchi, T.; Washington, J.; Kubiak, C. P., Effects of rapid intramolecular electron transfer on vibrational spectra. *Science* **1997,** *277* (5326), 660-663.

24. Zhang, L. T.; Zhu, X. Q.; Hu, S. M.; Zhang, Y. X.; Su, S. D.; Yang, Y. Y.; Wu, X. T.; Sheng, T. L., Influence of ligand substitution at the donor and acceptor center on MMCT in a cyanide-bridged mixed-valence system. *Dalton T* **2019,** *48* (22), 7809-7816.

25. Zhang, L.-T.; Zhu, X.-Q.; Su, S.-D.; Yang, Y.-Y.; Hu, S.-M.; Wen, Y.-H.; Wu, X.-T.; Sheng, T.-L., Influence of the Substitution of the Ligand on MM'CT Properties of Mixed Valence Heterometallic Cyanido-Bridged Ru–Fe Complexes. *Crystal Growth & Design* **2018,** *18* (6), 3674-3682.

26. Bignozzi, C. A.; Indelli, M. T.; Scandola, F., Bis(2,2'-Bipyridine)Ruthenium(Ii)-Hexacyanochromate(Iii) Chromophore Luminophore Complexes - Intramolecular Energy-Transfer, Excited-State Intervalence Transfer, and Doublet Doublet Annihilation. *Journal of the American Chemical Society* **1989,** *111* (14), 5192-5198.

27. Kwon, O.; Barlow, S.; Odom, S. A.; Beverina, L.; Thompson, N. J.; Zojer, E.; Bredas, J. L.; Marder, S. R., Aromatic amines: a comparison of electron-donor strengths. *J Phys Chem A* **2005,** *109* (41), 9346-52.

28. Yang, Y. Y.; Zhu, X. Q.; Hu, S. M.; Su, S. D.; Zhang, L. T.; Wen, Y. H.; Wu, X. T.; Sheng, T. L., Different Degrees of Electron Delocalization in Mixed Valence Ru-Ru-Ru Compounds by Cyanido-/Isocyanido-Bridge Isomerism. *Angew Chem Int Ed Engl* **2018**, 14046-14050.

29. Winter, R. F., Half-Wave Potential Splittings Delta E-1/2 as a Measure of Electronic Coupling in Mixed-Valent Systems: Triumphs and Defeats. *Organometallics* **2014,** *33* (18), 4517-4536.

30. D'Alessandro, D. M.; Keene, F. R., Current trends and future challenges in the experimental, theoretical and computational analysis of intervalence charge transfer (IVCT) transitions. *Chem. Soc. Rev.* **2006,** *35* (5), 424-440.

31. Sheng, T. L.; Vahrenkamp, H., Long range metal-metal interactions along Fe-NC-Ru-CN-Fe chains. *Eur J Inorg Chem* **2004,** (6), 1198-1203.

32. Ma, X.; Lin, C. S.; Hu, S. M.; Tan, C. H.; Wen, Y. H.; Sheng, T. L.; Wu, X. T., Influence of Central Metalloligand Geometry on Electronic Communication between Metals: Syntheses, Crystal

Structures, MMCT Properties of Isomeric Cyanido-Bridged Fe2Ru Complexes, and TDDFT Calculations. *Chemistry-a European Journal* **2014,** *20* (23), 7025-7036.

33. Scandola, F.; Argazzi, R.; Bignozzi, C. A.; Chiorboli, C.; Indelli, M. T.; Rampi, M. A., Electronic coupling between remote metal centers in cyanobridged polynuclear complexes. *Coordin Chem Rev* **1993,** *125* (1-2), 283-292.

34. Kubiak, C. P., Inorganic electron transfer: sharpening a fuzzy border in mixed valency and extending mixed valency across supramolecular systems. *Inorg Chem* **2013,** *52* (10), 5663-76.

35. Kentaro Mishiba; Masanori Ono; Tanaka, Y.; Akita, M., A Fully Charge-Delocalized 2-Dimensional Porphyrin System with Two Different Class III States. *Chemistry - A European Journal* **2017,** *23* (9), 2067-2076.

36. Ma, X.; Hu, S. M.; Tan, C. H.; Zhang, Y. F.; Zhang, X. D.; Sheng, T. L.; Wu, X. T., From antiferromagnetic to ferromagnetic interaction in cyanido-bridged Fe(III)-Ru(II)-Fe(III) complexes by change of the central diamagnetic cyanido-metal geometry. *Inorg Chem* **2013,** *52* (19), 11343-50.

37. Rossi, M. B.; Piro, O. E.; Castellano, E. E.; Albores, P.; Baraldo, L. M., Reactivity and spectroscopy of the {Ru(DMAP)(5)) fragment: An {Ru(NH3)(5)} analogue. *Inorg Chem* **2008,** *47* (7), 2416-2427.

38. Mazur, S.; Sreekumar, C.; Schroeder, A. H., Symmetry Vs Fluxionality, a Radical-Anion with Borderline Properties. *Journal of the American Chemical Society* **1976,** *98* (21), 6713-6714.

39. Coat, F.; Lapinte, C., Molecular wire consisting of a C-8 chain of elemental carbon bridging two metal centers: Synthesis and characterization of [{Fe(eta(5)-C(5)Me(5))(dppe)}(2)(mu-C-8)]. *Organometallics* **1996,** *15* (2), 477-479.

40. Magnuson, R. H.; Taube, H., Mixed Oxidation States in Osmium Ammine Dinitrogen Complexes. *Journal of the American Chemical Society* **1972,** *94* (20), 7213-&.

41. Wu, R.; Koske, S. K. A.; White, R. P.; Anson, C. E.; Jayasooriya, U. A.; Cannon, R. D., Electron transfer rates in a trinuclear mixed-valence iron(III, III, II) molecule: a variable-temperature infrared spectroscopic study. *Journal of the Chemical Society, Chemical Communications* **1994,** (14).

42. Porter, T. M.; Heim, G. P.; Kubiak, C. P., Stable Mixed-Valent Complexes Formed by Electron Delocalization Across Hydrogen Bonds of Pyrimidinone-Linked Metal Clusters. *Journal of the American Chemical Society* **2018,** *140* (40), 12756-12759.

43. Cheng, T.; Shen, D. X.; Meng, M.; Mallick, S.; Cao, L.; Patmore, N. J.; Zhang, H. L.; Zou, S. F.; Chen, H. W.; Qin, Y.; Wu, Y. Y.; Liu, C. Y., Efficient electron transfer across hydrogen bond interfaces by proton-coupled and -uncoupled pathways. *Nat Commun* **2019,** *10* (1), 1531.

44. Xiao Ma; Chen-Sheng Lin; Xiao-Quan Zhu; Sheng-Min Hu; Tian-Lu Sheng; Xin-TaoWu, a., An Unusually Delocalized Mixed-Valence State of a Cyanidometal-Bridged Compound Induced by Thermal Electron Transfer. *Angew Chem Int Edit* **2017,** *56* (6), 1605–1609.

45. Ito, T.; Hamaguchi, T.; Nagino, H.; Yamaguchi, T.; Kido, H.; Zavarine, I. S.; Richmond, T.; Washington, J.; Kubiak, C. P., Electron transfer on the infrared vibrational time scale in-the mixed valence state of 1,4-pyrazine- and 4,4 '-bipyridine-bridged ruthenium cluster complexes. *Journal of the American Chemical Society* **1999,** *121* (19), 4625-4632.

46. Webb, R. J.; Rheingold, A. L.; Geib, S. J.; Staley, D. L.; Hendrickson, D. N., Pronounced Anion Dependence of Valence Detrapping Temperature in Mixed-Valence 1',1'''-Disubstituted Biferrocenium Salts. *Angewandte Chemie-International Edition in English* **1989,** *28* (10), 1388-1390.

47. Webb, R. J.; Geib, S. J.; Staley, D. L.; Rheingold, A. L.; Hendrickson, D. N., Mixed-Valence Biferrocenes - Pronounced Anion Dependence of Valence Detrapping and Effects of an Asymmetric Crystal-Lattice. *Journal of the American Chemical Society* **1990,** *112* (13), 5031-5042.

48. Aguirre-Etcheverry, P.; O'Hare, D., Electronic Communication through Unsaturated Hydrocarbon Bridges in Homobimetallic Organometallic Complexes. *Chem Rev* **2010,** *110* (8), 4839-4864.
49. Geiss, A.; Kolm, M. J.; Janiak, C.; Vahrenkamp, H., M(mu-CN)Fe(mu-CN)M' chains with phthalocyanine iron centers: Redox, spin-state, and mixed-valence properties. *Inorg Chem* **2000,** *39* (18), 4037-4043.
50. Le Narvor, N.; Toupet, L.; Lapinte, C., Elemental Carbon Chain Bridging Two Iron Centers: Syntheses and Spectroscopic Properties of [Cp*(dppe)Fe-C4-FeCp*(dppe)]n+.cntdot.n[PF6]-. X-ray Crystal Structure of the Mixed Valence Complex (n = 1). *Journal of the American Chemical Society* **1995,** *117* (27), 7129-7138.
51. Guo, Z. H.; Jin, Z. X.; Wang, J. Y.; Pei, J., A donor-acceptor-donor conjugated molecule: twist intramolecular charge transfer and piezochromic luminescent properties. *Chem Commun (Camb)* **2014,** *50* (46), 6088-90.
52. Amthor, S.; Lambert, C.; Dummler, S.; Fischer, I.; Schelter, J., Excited mixed-valence states of symmetrical donor-acceptor-donor pi systems. *J Phys Chem A* **2006,** *110* (15), 5204-14.
53. Launay, J. P.; Babonneau, F., Semi-Classical Model of a Trinuclear Mixed-Valence System. *Chem Phys* **1982,** *67* (3), 295-300.
54. Ondrechen, M. J.; Ko, J.; Zhang, L. T., A Model for the Optical-Absorption Spectrum of (Mu-Pyrazine)Decaamminediruthenium(5+) - What Hath Creutz and Taube Wrought. *Journal of the American Chemical Society* **1987,** *109* (6), 1672-1676.
55. Brunschwig, B. S.; Creutz, C.; Sutin, N., Optical transitions of symmetrical mixed-valence systems in the Class II-III transition regime. *Chem. Soc. Rev.* **2002,** *31* (3), 168-184.
56. Glover, S. D.; Kubiak, C. P., Persistence of the Three-State Description of Mixed Valency at the Localized-to-Delocalized Transition. *Journal of the American Chemical Society* **2011,** *133* (22), 8721-8731.
57. Zoerb, M. C.; Harris, C. B., A Simulation Program for Dynamic Infrared (IR) Spectra. *J Chem Educ* **2013,** *90* (4), 506-507.
58. Sil, A.; Ghosh, U.; Mishra, V. K.; Mishra, S.; Patra, S. K., Synthesis, Structure, Electrochemical, and Spectroscopic Properties of Hetero-Bimetallic Ru(II)/Fe(II)-Alkynyl Organometallic Complexes. *Inorg Chem* **2019,** *58* (2), 1155-1166.